ACS OMEGA

Open Access

http://pubs.acs.org/journal/acsodf

Article

Preparation of Low-Viscosity Epoxy Resin Sealing Agent and Evaluation of Injection, Plugging, and Degradation Properties

Yadong Chen, Yongming Li,* Yu Peng, Dingyuan Zhang, Jiandu Ye, and Youshi Jiang

Cite This: *ACS Omega* 2024, 9, 19992−20002

Read Online

ACCESS | Metrics & More | Article Recommendations

ABSTRACT: The technology of water plugging and increasing production in high water cut reservoirs of low permeability is a common problem in the industry. Epoxy resin, displaying excellent mechanical properties and adherent performance, can easily inject a tiny crack, forming a long-term blocking barrier. This study aimed to investigate an easily injectable degradable epoxy resin sealing material. The injectable performance, long-term stability, and mechanical and plugging properties were comparatively analyzed in the fractured core, and the degradable performance was discussed in the degrading solution. The result showed that the range of *R* (*R* is the ratio of EOG and MHHPA) from 1 to 1.1 and the mass fraction range of EMI from 0.01 to 4 wt % are the optimal formulations (EOGM). The curing time from 1 to 12 h could be regulated by adjusting the dosage of EMI, as well as the strength being more than 60 MPa. The plugging agent's initial viscosity is lower than 100 MPa s at 20 °C and injecting pressure is lower than 0.1 MPa. After curing for 24 h, compressive strength was more than 72.76 MPa, 3.6 times higher than that of cement, and the adhesion strength was 4.41 MPa when the contact area was 75.93 cm^3. Breakthrough pressures for sealing 1−5 mm fractures were all more than 10 MPa, and the breakthrough pressure for 1 mm crack even reached 29.4 MPa. Epoxy resin/acid anhydride system could be degraded in a mixed solution of phenol−potassium salt−heavy aromatics within 7 days at 60−100 °C, which reduced the plugging well risk of the epoxy resin plugging agent. These results suggest that an epoxy resin/acid anhydride plugging agent can be employed effectively and safely for the injection of tiny cracks, which is of great engineering significance.

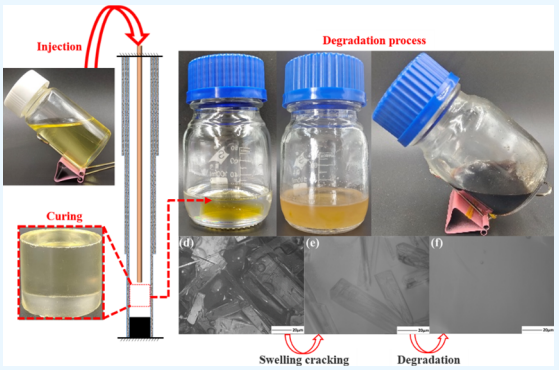

INTRODUCTION

Due to a long period of water injection development, the high water production rate has hampered the development of the oil and gas industries in recent years.[1−3] The oil and gas reservoirs formed the high-permeability regions after the long-term injection of water, resulting in the lower mechanical energy utilization rate of the injected water and oil and gas production rate.[4,5] Moreover, other reasons that caused the high water production rate included cement sheath failure and channeling flow outside the horizontal well tube.[6−9] Globally, the annual water production rate of oil and gas reservoirs increased each year, which considerably restricted the stabilization and increase in oil field production. About 3−4 tons of water was produced per ton of oil produced, and old oil fields produced more water. The average water content per ton of oil was usually more than 8 tons.[10]

The technology of water plugging and increasing production in high water cut reservoirs of low permeability is a common problem in the industry.[1,11] To enormously increase reservoir production, the composite technology of water plugging and fracturing by plugging first water breakthrough reservoirs and then fracturing new fractures was proposed, which is beneficial to long-term stable production. However, with the continuous advancement of field execution, it was believed that the plugging agent was critical, and its comprehensive performance plays a crucial role in the application process.[12] Nowadays, the commonly used plugging materials, such as inorganic gels, organic gels, and cement, for external sealing of horizontal well casing channeling, casing damage repair of oil and gas wells, and sealing the high moisture content well during the construction of the repeated fracturing had the following problems:[13−16] (1) The conventional plugging agent was diluted easily by oil or formation water to induce the ineffectiveness of water plugging. (2) The driven water readily broke through the sealing zone for the low adhesion strength agent and the surface layer of casing pipes, cement sheaths, and rocks. (3) The long-term plugging performance was poor due to the easy inorganic gel of the water loss and likely curing shrinkage cement plugging agent. (4) The

Received: December 15, 2023
Revised: March 30, 2024
Accepted: April 2, 2024
Published: April 26, 2024

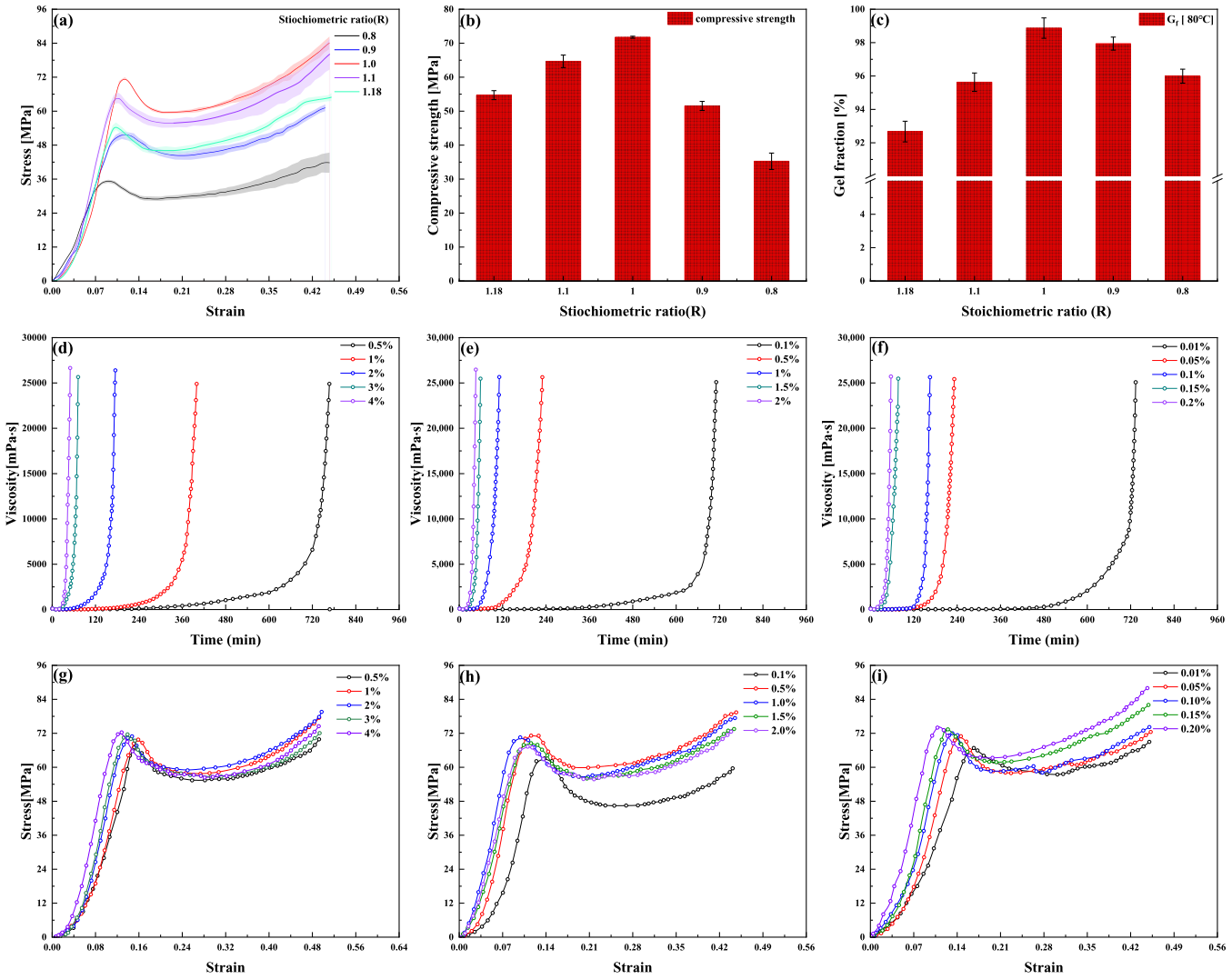

Figure 1. Optimization of the dosage of curing agent and accelerator. (a) Stress−strain curves with different values of *R*; (b) rupturing stress; (c) gel fraction with different values of *R*; (d)−(f) rheology of resin plugging agents; (g)−(i) stress−strain curves with dosages of different accelerators.

blockage material was hard to remove after the construction troubles of pipe stuck while injecting cement.[6,17−19] A considerable amount of literature on the application of epoxy resins is available, such as repairing damaged cement sheaths and casing damaged wells, treating sand production problems, and plugging highly permeable passages. However, there are a variety of challenges associated with the application of resins to repairing well operation, such as alternating loads from both the sustained casing pressure and corrosion of the resin by chemicals could have an impact on the long-term stability of the resin.[20−23]

Epoxy resin is a kind of thermosetting material. The free-flowing polymer solution in conventional form cures and forms an irreversible rigid solid under reservoir temperature conditions after being pumped into the formation. Compared to systems such as cement, organic gels, and inorganic gels, epoxy resin plugging agents are an excellent solution to repairing well operation, owing to the low elastic modulus, high compressive strength, resistance to chemical corrosion, high permeability, low rheological capacity, excellent mechanical properties, and adjustable compressive strength and thickening time.[24] Epoxy resin was usually applied to long-term reservoir management owing to premature curing of the epoxy resin during the construction process and blockage of the tubing or annulus, leading to the shutdown of the well. It is necessary to study the degradation properties of resin-plugging agents to extend the execution application. The main degradation methods include heat treatment and chemical degradation.[25,26] Chemical degradation is the use of chemical solvents to degrade epoxy composites;[27] several common chemical solvents include tetrahydronaphthalene, nitric acid, supercritical/subcritical alcohols, and supercritical/subcritical water.[25,28−35] Liu proposed a chemical degradation method using supercritical water as a solvent and phenol and KOH as catalysts, where phenol and potassium ions showed a synergistic effect and promoted the degradation rate of the resin.[33] Wang proposed a milder degradation method using phenol as a solvent and K_2CO_3 as a catalyst to degrade the resin at lower temperatures.[36] However, the long chemical degradation time of epoxy resin and the small contact area between the plugging agent and the degrading agent increase the difficulty of degradation of the plugging agent.[37] However, the chemical degradation time of epoxy resin is long, and the contact area between the plugging agent and the degradation agent is small, which improve the degradation difficulty of the plugging agent. Besides, chemical solvents under critical conditions need specific environmental temperatures and pressure, but nitric acid is corrosive to piping, and

https://doi.org/10.1021/acsomega.3c10034
ACS Omega 2024, 9, 19992−20002

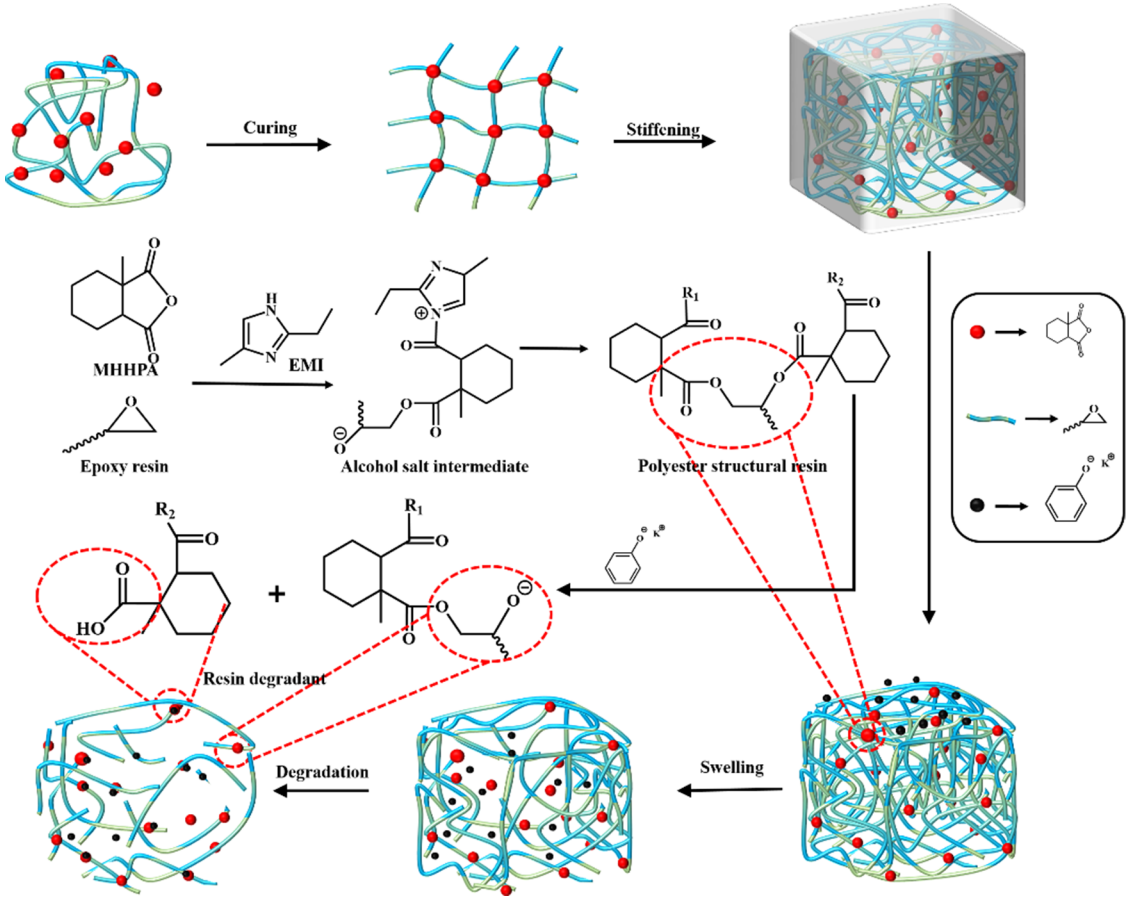

Figure 2. Curing mechanism diagram of EOGM.

tetrahydronaphthalene solvents are expensive. The degradation methods are harsh to be utilized in oilfield production.

In this work, a low-shrinkage, high-strength epoxy resin plugging agent was prepared based on a low-viscosity petroleum-based epoxy resin, and the curing agent and accelerator dosage were optimized, and the performance of injectable, mechanical, adhesion, and plugging was evaluated. According to the curing mechanism of the epoxy resin plugging agent, a degradation solution was prepared, which can degrade epoxy resin at a constant temperature in medium- and low-temperature reservoirs. To further investigate the effect of temperature degradation of the resin plugging agent in the degradant, we investigated the degradation effect of the epoxy resin of potassium salt concentration and temperature and the curing degradation mechanism of resin by combining with infrared experiments.

RESULTS AND DISCUSSION

Optimization and Characterization of Matrix Formulation and Curing Parameters. *Optimized Hardener and Accelerator Concentration.* The curing reaction mechanism of EOGM imidazole-promoted epoxy resin with acid anhydride has been widely investigated, and the performance of epoxy resin is inextricably linked to the amount of hardener and accelerator; therefore, it is necessary to examine the amount of hardener and accelerator. Samples 1 to 5 in Table 3 were prepared to investigate the dosage of MHHPA on the performance of compressive strength and gel fraction, in which the stoichiometric ratio of anhydride/epoxy resin (R) is 0.8, 0.9, 1, 1.1, and 1.18, respectively. Figure 1a shows that the stress−strain relationship can be divided into three parts. The first part is the elastic deformation stage. It is the interval from the origin of the stress−strain curve to the peak point before rupturing that is approximately linear and indicates that the elastic deformation occurs under the action of the applied load. The cured resin did not undergo necking. The second part is the necking stage, with a more complex force. The compressive strength of this stage decreases under a uniform load, and the cured resin does not rupture. The third part is the resin destruction stage, and after the reverse bending point, the compressive strength increases with an increase in the applied load, and the cured resin may rupture during this process.[37,38] In summary, the maximum compressive strength should be the first peak of the curve. Figure 1a,b shows that the compressive strength is greater than 60 MPa when in the interval R = 1 to 1.18, where the compressive strength at a strain rate of 0.117 is 71.76 MPa when R = 1, which is mainly due to the high degree of reaction of the epoxy group with the anhydride.

Figure 1c shows that the gel fraction is 98.87% when R = 1 and at the maximum gel density of the resin plugging agent. The peak value of the compressive strength decreases when the R value is lower than or higher than 1 because a lower anhydride dosage results in inadequate curing. In addition, a higher anhydride dosage occupies some of the reaction sites. Both of these lead to a decrease in the reaction efficiency of the epoxy groups, as reflected in Figure 1c, which shows that either too low or too much anhydride dosage results in a reduction of the gel fraction.[39]

https://doi.org/10.1021/acsomega.3c10034
ACS Omega 2024, 9, 19992−20002

Due to the construction conditions in various oilfields needing different curing times, it is necessary to examine the viscosity change during the injection process.[40] Figure 1d−f shows the viscosity−time curves of different accelerator dosages at 60, 80, and 100 °C. The initial viscosities of the solutions are all lower than 100 mPa s. Curing time could be controlled in 1−12 h by adjusting the concentration of the accelerator under the conditions of the reservoir temperature. Figure 1g−i shows the maximum compressive strength of the resins measured at 60, 80, and 100 °C after curing for 24 h with different accelerator dosages. The compressive strength could be regulated by adjusting the reaction accelerator dosage at 60 to 100 °C.[41] To summarize, high compressive strength properties can be realized in the reservoir environment of 60−100 °C when the range of *R is* from 1 to 1.1 and the mass fraction range of the accelerator is from 0.01 to 4 wt %.

Characterization of the Solidification and Degradation Mechanisms. Figure 2 shows the curing and degradation processes. The curing reaction of the nucleophilic accelerator−anhydride−epoxy system is commonly regarded as a two-stage reaction. The first stage of the reaction is the formation of a carboxylate anion from the binding reaction of the promoter with the epoxy group. The second stage of the reaction is the reaction of the alkoxide anion with the epoxy group to form the carboxylic acid anion again. Finally, a three-dimensional polyester structural material with degradable properties is formed.[38] As shown in Figure 2, the synergistic effect of phenol and K^+ favors the degradation of the ester bond to an oligomeric solution, which increases the rate of plugging agent degradation and provides the possibility of low-temperature degradation of EOGM.

Figure 3 shows the infrared spectrum of the EOGM reaction solution, EOGM, and the EOGM degradation solution. In the

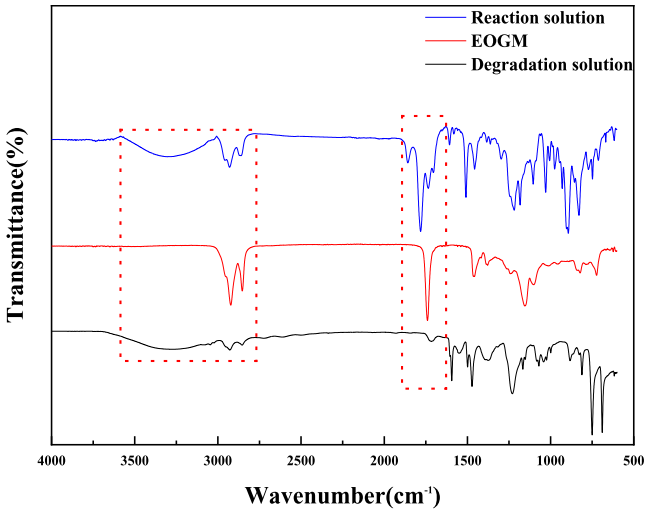

Figure 3. Infrared spectra of EOGM reaction solution, EOGM, and EOGM degradation solution.

infrared spectrum, 3270.2 and 1781.34 cm^{-1} are the absorption characteristic peaks of −COOH; 1218.75 and 829.51 cm^{-1} are the absorption characteristic peaks of the epoxy group; and 1735.1 cm^{-1} is the absorption characteristic peak of C═O. In the infrared spectrum of EOGM, the characteristic peaks of absorption of −COOH at 3270.2 and 1781.34 cm^{-1} and that of epoxy groups at 1218.75 and 829.51 cm^{-1} disappeared, and the characteristic peak of C═O at 1740.1 cm^{-1} enhanced, which indicated that the epoxy resin reacted with the anhydride to form the polyester structure of the EOGM resin. The infrared spectrum of the EOGM degradation solution showed an enhancement of the characteristic peak of −OH at 3354.23 cm^{-1} and a significant decrease in the intensity of the characteristic peak at 1722.89 cm^{-1}, indicating the degradation of the polyester structure. In conclusion, the reaction of the epoxy resin with MHHPA produced an EOGM plugging agent and degraded under the action of a degradation agent.[33,42,43]

Injection Properties. Injection properties are the key of EOGM to plug microholes and microcracks. Figure 4a shows the initial viscosities of 5679, 384, 96, and 48 mPa s, respectively, for different diluent dosages at the temperature of 25 °C. The initial viscosities of sample 8 decreased with the increase in the dosage of the diluent. The test temperature was increased to 60 °C within 10 min, and the viscosity stabilization time is more than 60 min after heating up to 60 °C, indicating EOGM has excellent flow properties. The effect of diluent dosage on the injection properties was investigated using a steel crack core with 1 mm width, and the injection stabilization pressures of the samples with different diluent dosages were 0.28, 0.12, 0.10, and 0.07 MPa, respectively. With the increase of the diluent dosage, the liquid flow performance was enhanced, the injection pressure was reduced, and the tiny cracks could be easily immersed. Figure 4 shows that with the increase in the diluent dosage, the longer the low-viscosity period, the better would be the injection stability. The initial viscosity of E51 is 98 mPa s, and the diluent ratio is 10:2; the stabilization interval is greater than 60 min; and the stabilization of the injection pressure is 0.1 MPa. The viscosity−temperature curve of Figure 1d−f also conforms to this rule, which indicates that EOGM has excellent fluidity and injection properties.

Analysis of Adaptive Plugging Performance. *Stability Performance of EOGM.* The plugging agent needs to have excellent thermal stability due to the high temperature in the reservoir. Hence, the thermal gravity of EOGM was investigated in Figure 5a. It shows that the EOGM decomposes in the temperature range of 150−500 °C. The thermal decomposition of EGOM was categorized into two stages. According to the TG-DTG curves, the first stage was in the temperature interval from 147.59 to 262.08 °C with a mass loss of 9.83%; the second stage was in the temperature interval from 262.08 to 600 °C with a mass loss of 86.54%. In the temperature interval from 147.59 to 262.08 °C, the low-molecular components of the plugging agent were separated by heat, and the temperature interval from 262.08 to 600 °C is the decomposition stage of the EOGM plugging agent. When the temperature was 600 °C, the remaining mass of the plugging agent was 3.63%. Figure 5a shows that the EOGM plugging agent has excellent thermal stability at 30−140 °C, which satisfies the needs of oilfield plugging. Figure 5b,c shows the mass retention of the EOGM after 30 days of one-sided immersion in 10% hydrochloric acid, alkaline fracturing fluid at pH 9−10, and simulated formation water (salinity is 6×10^4 mg/L). The mass loss after 30 days of immersion was 0.049 and 0.237%, respectively, and its weight loss was considered negligible, indicating that EOGM has excellent long-term stability of blocking performance in harsh formation environments.[44,45]

Mechanical Performance of EOGM. The plugging agent is mainly affected by the flooding pressure and fracture closure pressure when the formation is plugged. Hence, the curing shrinkage and compression rupture of the plugging agent are the main reasons for the failure of plugging in the reservoir.[46,47]

https://doi.org/10.1021/acsomega.3c10034
ACS Omega 2024, 9, 19992−20002

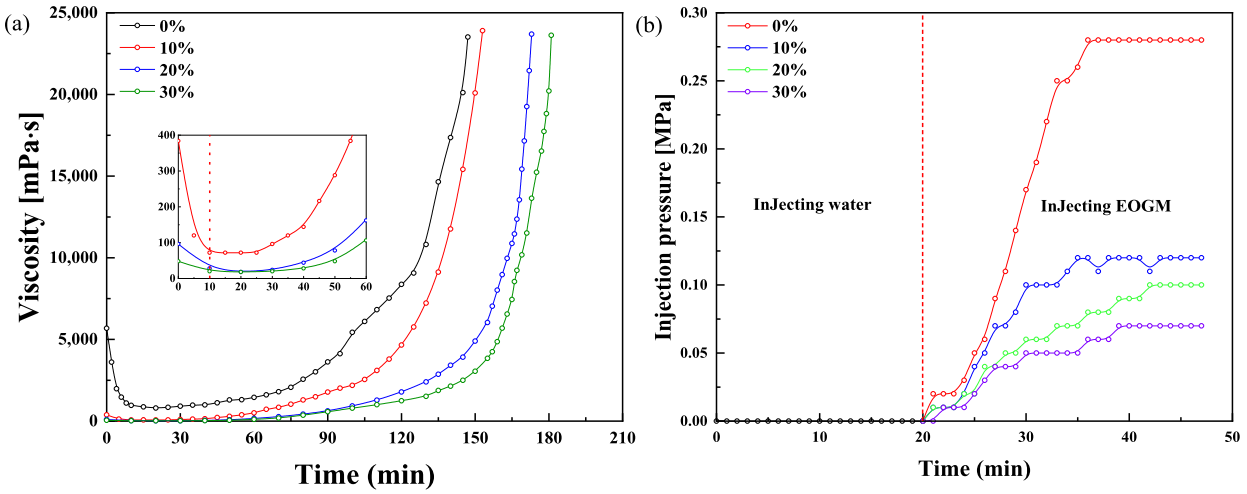

Figure 4. Relationship of the diluent dosage with the viscosity and injection property of the EOGM system. (a) Effect of diluent dosage on the viscosity−temperature curve. (b) Effect of diluent dosage on the injection performance.

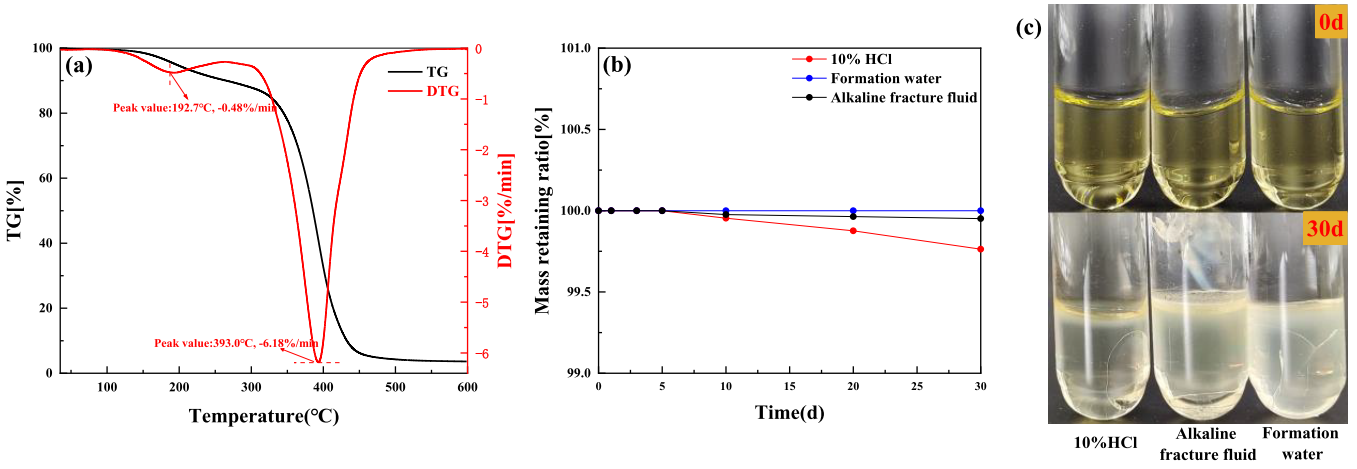

Figure 5. Stability performance of EOGM. (a) Thermal gravity curve of EOGM; (b) curve of compressive strength and mass retention rate at different aging times; (c) diagram at different aging times.

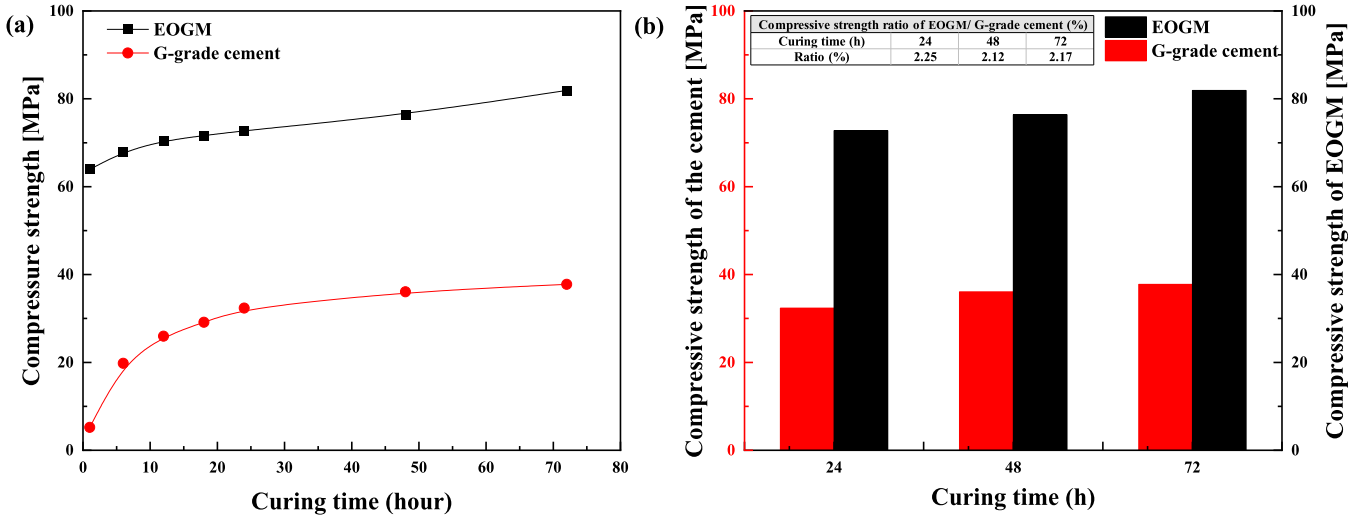

Figure 6. Compressive strength test. (a) Effect of curing time on the compressive strength of EOGM and G-grade cement. (b) Ratio of compressive strength of EOGM and G-grade cement for 24, 48, and 72 h curing time.

Figure 6a shows the increase in compressive strength of EOGM with increasing curing time at 80 °C. The compressive strengths after 24, 36, and 72 h of curing were 72.76 76.38, and 81.9 MPa, respectively. Figure 6b shows the compressive

https://doi.org/10.1021/acsomega.3c10034
ACS Omega 2024, 9, 19992−20002

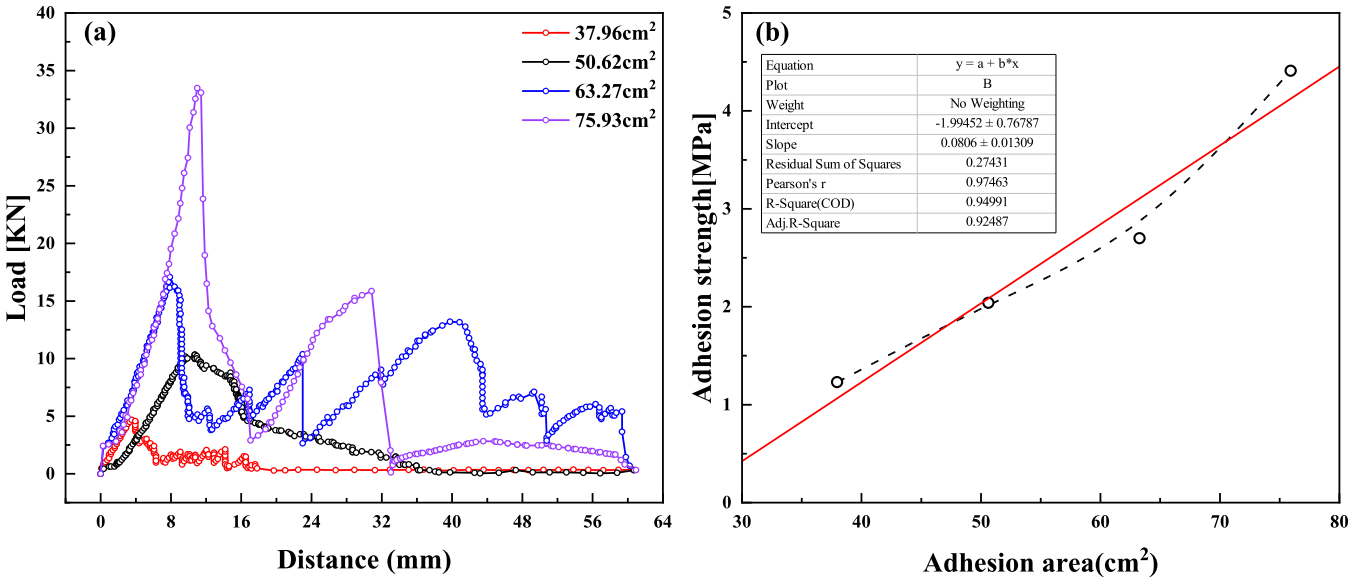

Figure 7. Effect of contact area on the adhesion properties of EOGMs under curing for 24 h. (a) Load−displacement curve. (b) Relationship between the cemented area and adhesion strength.

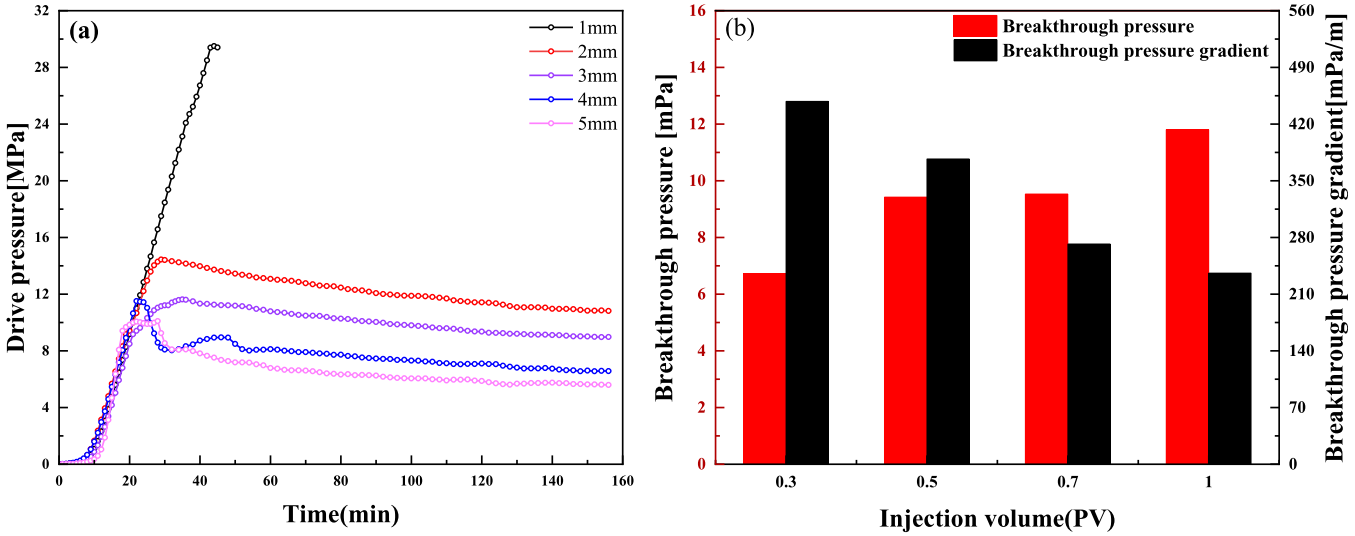

Figure 8. Plugging performance of the EOGM. (a) Plugging performance on different fracture widths; (b) breakthrough pressure and breakthrough pressure gradient for plugging with different fracture widths.

strength of EOGM and G-grade cement slurry, respectively. The compressive strength is 2.25 times that of G-grade cement after curing for 24 h. Besides, the compressive strength of EOGM gradually increased with the extension of curing time. The above results show that the EOGM has an excellent compressive strength. Effective sealing zones and long-term stable sealing zones can be formed quickly during the formation.

The adhesion performance of the EOGM can be characterized by its interfacial bond strength (Figure 10). Figure 7 shows the load−displacement curves for different contact areas of the EOGM with the wall, and the adhesion strength was obtained by eq 2 calculations. The load increases with the increase of the contact area between the resin and the wall, and the adhesion strength and adhesion strength gradient are consistent with the change rule of the load. When the adhesive area was 75.93 cm^2, the adhesion strength was 4.41 MPa, which shows excellent resistance to the uniaxial force of water−flood displacement and injected fracturing fluids.

Plugging Performance of EOGM. The plugging performance of EOGM in fractures was investigated by steel fracture core displacement experiments. Figure 8a shows the sealing performance of EOGM for steel cores with different fracture widths; the fracture width is between 1 and 5 mm, and all fracture breakthrough pressures were more than 10 MPa; the narrower the fracture, the greater is the sealing strength. The breakthrough pressure of the 1 mm fracture is 29.5 MPa, approximately 2.04 times higher than 2 mm fracture, indicating that the EOGM has excellent plugging performance for tiny fractures. Figure 8b shows the plugging performance of steel cores with 3 mm fracture width for different EOGM injection volumes (PV), which indicates that the greater the PV volume, the greater is the strength of the blocking and the smaller the breakthrough pressure gradient. When the injected PV volume is higher than 0.5 PV, the breakthrough pressure gradient decreases with the increase in PV volume, and the breakthrough pressure gradient ranges from 200 MPa/m to 400 MPa/m.

https://doi.org/10.1021/acsomega.3c10034
ACS Omega 2024, 9, 19992−20002

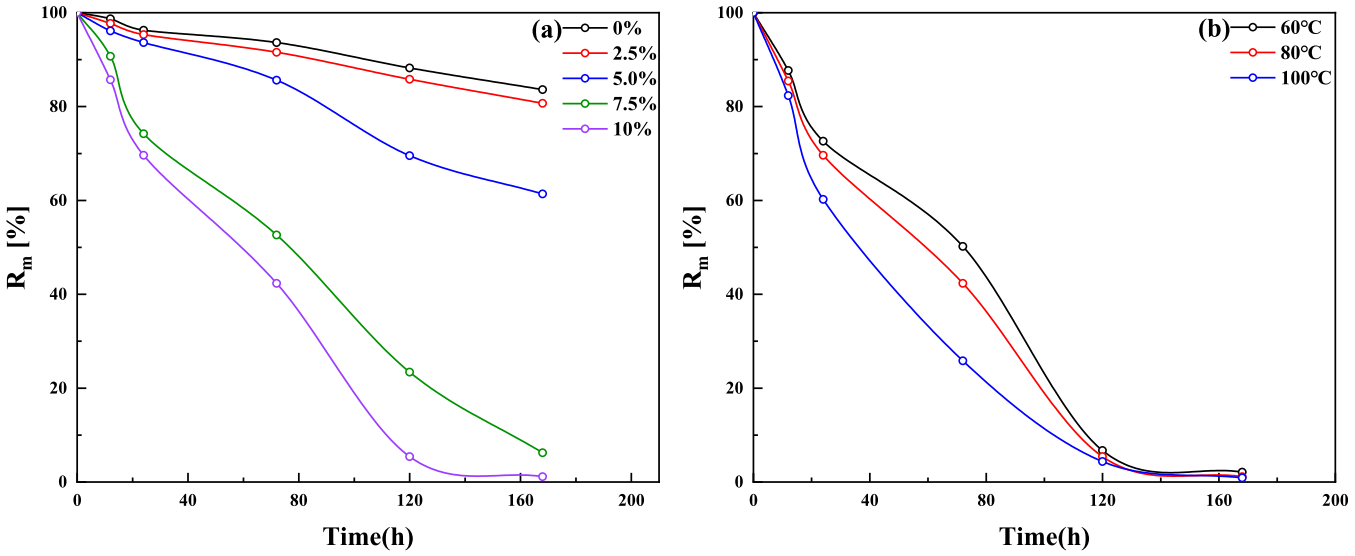

Figure 9. Degradation performance. (a) Effect of potassium carbonate solution concentration; (b) effect of temperature.

Table 1. Diagram of EOGM Degradation in Degradation Solution with Different K_2CO_3 Concentrations

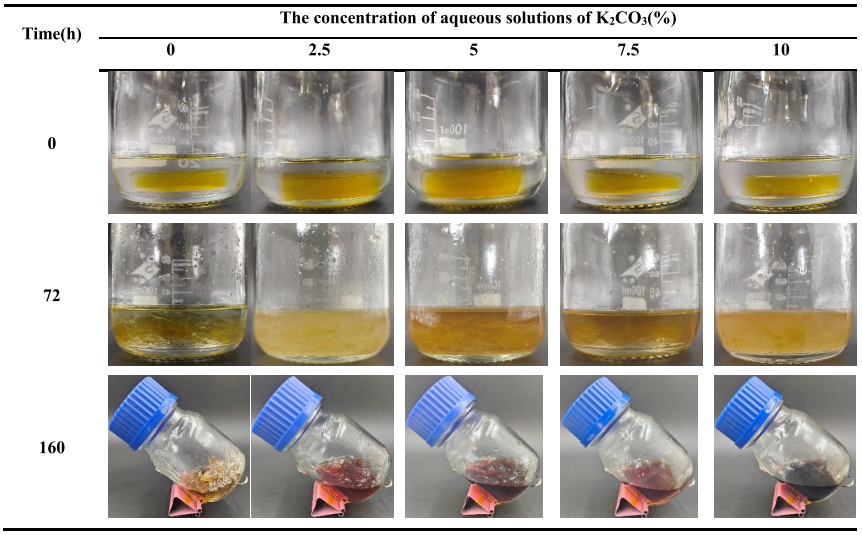

Figure 1d−i shows that EOGM has a stable low-viscosity stage in the range of 60−100 °C, with the resin viscosity below 100 mPa s and compressive strength greater than 60 MPa, and Figure 5 indicates EOGM resin solution below 100 mPa s, exhibiting excellent injectable performance. Figures 5−8 show that EOGM has excellent mechanical, long-term stability, and plugging properties, which can be suitable for low-permeability reservoirs with high water content well plugging.

Unblocking Performance. The cured plugging agent in the wellbore at the end of construction is a major safety hazard affecting subsequent construction. In this study, the degradation liquid system was prepared based on the epoxy/acid anhydride system, 10 wt % K_2CO_3 solution +45 wt % phenol +45 wt % heavy aromatic hydrocarbons. The degradation of EOGM can be divided into two processes: the EOGM plugging agent is first swelled in a heavy aromatic solution and fragmented into small pieces of EOGM; then, the pieces of EOGM are further split into micrometer-sized particles and rapidly degraded to oligomers by the promotion of oxonium anions. The oxonium anion is formed by the synergistic formation of potassium salts with phenol under certain temperature conditions, and therefore the potassium salt concentration affects the degradation rate of the resin.[48,49] In addition, the reservoir temperature affects the degradation rate of resin-plugging agents. Therefore, this paper investigated the effects of the potassium salt concentration and reaction temperature on the degradation properties of resin-plugging agents.

Figure 9a and Table 1 show the degradation of the EOGM in degradation solutions with different concentrations of K_2CO_3 at 80 °C. The degradation rate of the resin accelerates with an increasing K_2CO_3 concentration. When the concentration of K_2CO_3 solution is 7.5 to 10 wt %, the EOGM was dissolved and fragmented into small pieces after 72 h and degraded into solution after 160 h. The larger the concentration of K_2CO_3 was, the smaller was the volume of the split resin pieces. Figure 9b shows the effect of temperature on the degradation rate of the EOGM plugging agent, which investigates the degradation rate of EOGM in degradation solution with 10 wt % K_2CO_3 concentration at 60, 80, and 100 °C, respectively. The results showed that the EOGM mass residue ratio was 2.09, 1.13, and

https://doi.org/10.1021/acsomega.3c10034
ACS Omega 2024, 9, 19992−20002

Table 2. Ion Composition of Formation Water from Oil Field CQ-1

ion content (mg/L)								
K^+/Na^+	Ca^{2+}	Mg^{2+}	Cl^-	SO_4^{2-}	HCO_3^-	total salinity(mg/L)	viscosity (mPa s)	water type
21,682	2931	653	39,982	426	368	66,042	1	$CaCl_2$

0.89 wt % after 160 h, respectively; the higher the temperature, the more rapid was the degradation. The residual EOGM particles were small in size and could be discharged back to the ground with the degradation solution.

Figures 2 and 3 show that the oligomer undergoes mainly ester bond depolymerization to form low-molecular acids and alcohols. K_2CO_3 and phenol can form oxonium anion with the ability to accelerate the decomposition of polyester structure, which can accomplish the degradation of the resin within 6−7 days after plugging the well and is beneficial to guarantee the production efficiency of the oilfield. Table 1 also shows that the resin degradation process is divided into the swelling and degradation stages.

CONCLUSIONS

This work developed the low-viscosity and high-strength resin plugging agent using EOG, MHHPA, and EMI. The range of R (R is the ratio of EOG and MHHPA) from 1 to 1.1 and the mass fraction range of EMI from 0.01 to 4 wt % are the optimal formulations (EOGM). The curing time from 1 to 12 h could be regulated by adjusting the dosage of EMI in the range of 60−100 °C, as well as the strength was more than 60 MPa. The width of the crack is 1 mm, and the injection pressure of EOGM is 0.1 MPa, which can easily enter into the microseam and micropore to realize effective sealing. EOGM has excellent thermal stability in the range of 30−140 °C and long-term stability in simulated formation water, 10% hydrochloric acid, and alkaline fracturing fluids. The compressive strength of EOGM after curing for 24 h was 72.76 MPa, the adhesive strength was 4.41 MPa/0.00759 m^2, and the plugging strength of 1−5 mm cracks was more than 10 MPa. The smaller cracks with more excellent sealing performance can be suitable for low-permeability reservoirs with high water content well plugging. Degradation experiments indicate that the EOGM can be completely degraded into a solution to be discharged back to the ground after 160 h, which can avoid accident treatment caused by faulty operation. Therefore, this low-viscosity, high-strength resin plugging agent can be used in a variety of applications, such as wellbore management, sand cementing, and annular leakage.

EXPERIMENTAL DESCRIPTION

Materials. The epoxy resin (E51), *n*-butyl glycidyl ether, and methylhexahydrophthalic anhydride (MHHPA) were produced by Runxiang Co., Ltd. in Changzhou, China. Oilwell cement (class G cement) was purchased from Jiahua Special Cement Co., Ltd., Leshan, China. The Aromatics solvent was purchased from Shengli Oilfield Shengli Chemical Co., Ltd. in Shandong, China. 2-Ethyl-4-methylimidazole (2,4-EMI), sodium dodecyl sulfate (SDS), toluene, potassium oxalate, potassium carbonate, sodium carbonate, potassium chloride, potassium hydroxide, and phenol were purchased from Sinopharm Group Chemical Reagent Co., Ltd., China. All chemicals were used without further purification. The ion composition of the simulated formation water is shown in Table 2. All concentrations in this research are on a weight basis.

Sample Preparation. The EOG low-viscosity epoxy resin is made of E51 and *n*-butyl glycidyl ether with a mass ratio of 10:2. At 25 °C, the epoxy value of the EOG epoxy main agent is from 0.49 to 0.52, viscosity from 79 mPa s, and its specific gravity from 1.12 to1.14 g/cm^3. The epoxide equivalent weight was determined via titration (hydrogen bromide method) and was 198 [g/eq].

EOGM was used as prepared to investigate the curing and degradation mechanism, stability, and strength performance in oil and gas reservoirs. MHHPA, EOG, and 2,4-EMI were added to the sample bottle, respectively, and the mixture was stirred with an electric agitator (JB-80SH, Shaoxing Xiniu Instrument Technology Co., Ltd.) until the solution was mixed uniformly. To transform the mixture solution of uncured EOGM into a curable resin, it was heated up to 60−100 °C. The amounts of 2,4-EMI and MHHPA were varied systematically in order to evaluate the optimum mixing ratio. Details of the composition of the prepared samples are given in Table 3.

Table 3. Composition of the EOG, MHHPA, and 2,4-EMI (Low-Viscosity Epoxy Resin: Methylhexahydrophthalic Anhydride + 2-Ethyl-4-methylimidazole, $m_{EMI} = (m_{EOG} + M_{MHHPA}) \times$ wt %) Resin Samples

sample	EOG: MTHPA	stoichiometric ratio R [anhydride/epoxy]	temperature [°C]	EMI [wt %]
1	100:100	1:1.18	80	0.5
2	100:93	1:1.1	80	0.5
3	100:85	1:1	80	0.5
4	100:77	1:0.9	80	0.5
5	100:68	1:0.8	80	0.5
6	100:85	1:1	60	0.5
7	100:85	1:1	60	1
8	100:85	1:1	60	2
9	100:85	1:1	60	3
10	100:85	1:1	60	4
11	100:85	1:1	80	0.1
12	100:85	1:1	80	0.5
13	100:85	1:1	80	1.0
14	100:85	1:1	80	1.5
15	100:85	1:1	80	2.0
16	100:85	1:1	100	0.01
17	100:85	1:1	100	0.05
18	100:85	1:1	100	0.1
19	100:85	1:1	100	0.15
20	100:85	1:1	100	0.2

Methods. *Gel Fractions.* The swelling behavior of the samples was studied using a solvent impregnation method. The samples were immersed in toluene at room temperature for 48 h to dissolve the non-cross-linked parts. After being dried at 80 °C for 48 h, the weight of the dried sample was measured as W_1. The gel fraction (G_f) of the samples was determined by eq 1:

$$G_f = \frac{W_1}{W_0} \times 100\% \quad (1)$$

where G_f is the sample gel fraction; W_0 is the initial weight of the sample; and W_1 is the weight of the dried sample.

https://doi.org/10.1021/acsomega.3c10034
ACS Omega 2024, 9, 19992−20002

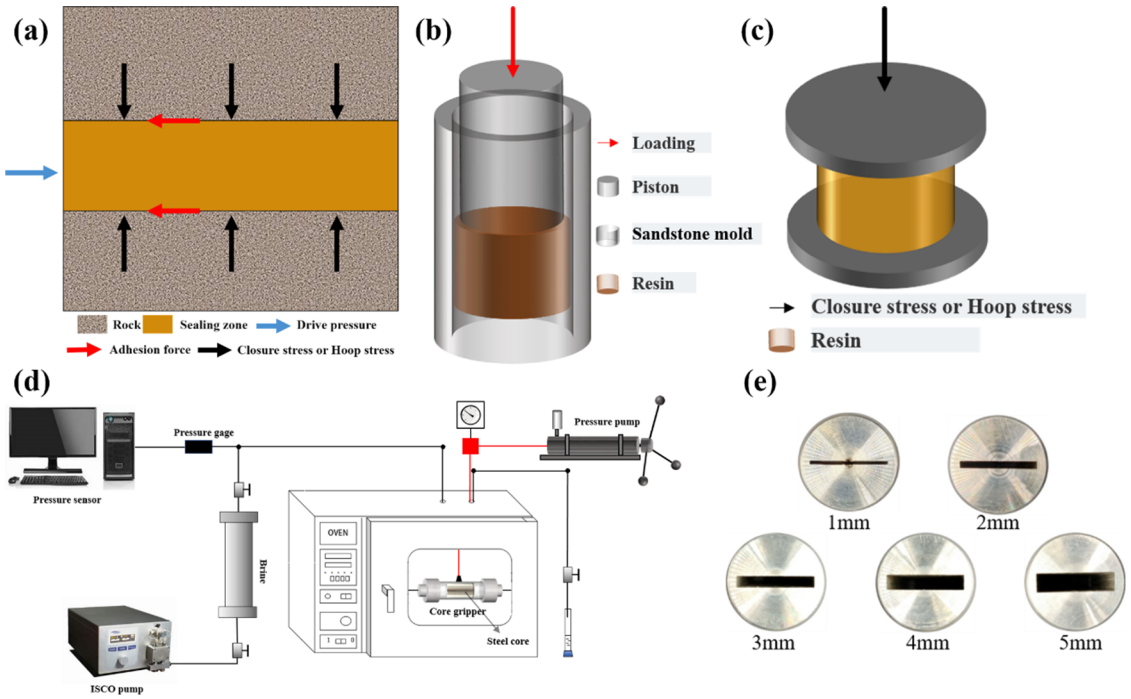

Figure 10. Mechanical properties' measurement diagram of the EOGM system: (a) Analysis of plugging agent force; (b) adhesion strength measurement; (c) compressive strength test; (d) displacement device; (e) steel fracture cores.

Characterizations. The infrared spectra (FT-IR) were recorded on a Thermo Nicolet 6700 spectrometer (Thermo Fisher Nicolet, America), and the absorbance mode was used. Thermogravimetric analysis (TGA) was performed by using a NETZSCH STA 449F3 thermogravimetric analyzer. Approximately 16 mg of the EOGM samples was placed in a nitrogen atmosphere of the velocity of 50 mL min^{-1}, and the temperature was raised from 50 to 600 °C at a heating rate of 10 °C min^{-1}.

Curing Time and Injection Properties. The viscosity−time curves of EOGM were measured by a DV-II digital viscometer (Brookfield, America). Weighted 50 g of EOGM solution was poured into 50 mL of a standard sample bottle and tested at predetermined temperatures (60, 80, and 100 °C). The shear rate was 50 r/min^{-1}, and the heat time was set as 10 min. Details as to the composition of curing time samples (Samples 6 to 20) are given in Table 3. The injection sample was prepared based on sample 8 (Table 3), and the dosage of *n*-butyl glycidyl ether was 0, 10, 20, and 30% of E51 of sample 8, respectively.

Long-Term Stability Measurements. The long-term stability refers to the performance of EOGM of acid, alkaline, and salt tolerance in a simulated reservoir environment. 5 g samples were weighed, put into ampules, and cured at 100 °C. Then, 10 g solutions, which were 10 wt % HCl solution, alkaline fracturing fluid (the range of pH is from 8 to 9), and formation water (6×10^4 mg/L), respectively, were added to those ampules, The long-term stability of EOGM could be directly reflected by the sample mass retain rate which is calculated based on the starting weight and the different aging time weights. The starting weight of all samples is designed as 5 g. The mass retention ratio was calculated by the mass ratios of different observation times on the initial mass.

Compressive Strength Measurements. According to Sample 8, 12, and 17 formulas (Table 3), samples were weighted and configured. 25 g samples were added in 40 × φ25 mm standard sample molds and cured for 1, 6, 12, 18, 24, 48, and 72 h at 80 °C, respectively. The standard sample was tested by a universal testing machine (UTM) to obtain the stress−strain curve.

Adhesive Strength Measurements. According to Sample 12 (Table 3), samples were weighted and configured. 84, 70, 56, and 42 g samples were added in 80 × φ40 mm standard sandstone mold, respectively. Piston test samples of 30, 40, 50, and 60 mm thickness were cured and prepared at 80 °C. The piston samples were tested by a UTM to obtain the load−time curve. The adhesive strength was calculated by eq 2.[24]

$$p = \frac{F}{S_c} = \frac{10F_s}{\pi hD} \tag{2}$$

where p is the adhesive strength of the resin−rock interface, MPa; F_S is load force, kN; S_c is the surface area of the cylinder, cm^2; h is the height of the resin, cm; D is the outer diameter of resin, cm.

Injectivity and Plugging Experiments. The core flooding experiment could reflect the plugging performance and afford a credible and scientific experimental basis for water blocking in the oil field. Figure 10d shows a schematic diagram of the core flooding experiment device. The steps of the experiments were as follows: (1) The simulated formation (Table 2) was used as the displacement of the fractured core; (2) Steel fractured core preparation. 50 mm × φ25 m cylindrical steel blocks were processed into fractured steel cores of different crack widths (the crack widths are 1, 2, 3, 4, and 5 mm, respectively). The steel core parameter is given in Table 4. Core flow research was conducted in a simulated reservoir condition at 80 °C. The fractured core was placed in a core clamper, and the experimental device was installed as shown in Figure 10d. The brine can be loaded into the intermediate storage container and energized by a plunger pump through the heating loop to the core clamper. Loading annulus pressure by the hand pump inspected the tightness of the device. The confining pressure should remain 2 MPa more than the setting drive pressure.

https://doi.org/10.1021/acsomega.3c10034
ACS Omega 2024, 9, 19992−20002

Table 4. Basic Parameters of Fractured Steel Cores[a]

core code	H_f (mm)	L_f (mm)	W_f (mm)	FV (mL)
1#	19.69	49.94	1.03	1.012
2#	19.87	50.00	2.04	2.026
3#	20.07	49.91	3.02	3.025
4#	20.09	49.98	4.09	4.107
5#	20.05	49.97	5.03	5.040

[a]H_f, fracture height; L_f, fracture length; W_f, fracture width; FV, fracture volume.

Subsequently, the core gripper remained in an oven at 80 °C to simulate the reservoir temperature. A stable flow velocity of brine was set as 1 mL min^{-1}. After stabilizing differential pressures, the displacement pressure and the liquid volume produced were recorded, respectively. The pressure difference between the two faces of the core was the measured data of the stable drive pressure. The injection speed of EOGM of Sample 2 (Table 3) steadily remained at 1 mL min^{-1}. The system was shut in for 24 h for the completion of the curing reaction at 80 °C. Then, the water injection direction was reversed. The flow velocity was set at 1 mL/min to displace the core. When the brine was displaced to another end, the displacement pressure was recorded.

Degradation Performance. According to Samples 8, 12, and 18 in Table 3, samples were weighted and configured, and 10 g samples were added in a 40 mm × φ25 m mold. Then, the prepared samples were transferred to 100 mL silk mouth bottles and degraded at 60, 80, and 100 °C, respectively. The mass retention ratio change over time was recorded. The mass retention ratio was calculated by eq 3

$$R_m = \frac{m_0 - m_i}{m_0} \times 100\% \quad (3)$$

where R_m is the mass retention ratio for different observation times, %; m_i is the residual mass at the observation time, g; m_0 is the initial mass, g.

AUTHOR INFORMATION

Corresponding Author

Yongming Li − *State Key Laboratory of Oil and Gas Reservoir Geology and Exploitation, Southwest Petroleum University, Chengdu 610500, China*; Email: swpifrac@163.com

Authors

Yadong Chen − *State Key Laboratory of Oil and Gas Reservoir Geology and Exploitation, Southwest Petroleum University, Chengdu 610500, China*; orcid.org/0009-0009-6690-6597

Yu Peng − *State Key Laboratory of Oil and Gas Reservoir Geology and Exploitation, Southwest Petroleum University, Chengdu 610500, China*

Dingyuan Zhang − *State Key Laboratory of Oil and Gas Reservoir Geology and Exploitation, Southwest Petroleum University, Chengdu 610500, China*

Jiandu Ye − *State Key Laboratory of Oil and Gas Reservoir Geology and Exploitation, Southwest Petroleum University, Chengdu 610500, China*

Youshi Jiang − *State Key Laboratory of Oil and Gas Reservoir Geology and Exploitation, Southwest Petroleum University, Chengdu 610500, China*

Complete contact information is available at: https://pubs.acs.org/10.1021/acsomega.3c10034

Author Contributions

Y.C.: Conceptualization, methodology, and writing—original draft. L.Y.: Writing, reviewing and editing, methodology, and conceptualization. Y.P.: Resources and visualization. J.Y.: Data curation and investigation. D.Z.: Experimental data. All authors analyzed the data and discussed the manuscript's results and conclusions. Y.C. and Y.L. contributed equally to this work.

Notes

The authors declare no competing financial interest.

ACKNOWLEDGMENTS

This work was supported by the National Natural Science Foundation of China (52174033), the National Natural Science Foundation of China (52304046), and the Natural Science Foundation of Sichuan Province (No. 2022NSFSC0971).

REFERENCES

(1) Yang, R.; Jiang, R.; Guo, S.; Chen, H.; Tang, S.; Duan, R. Analytical study on the Critical Water Cut for Water Plugging: Water cut increasing control and production enhancement. *Energy* **2021**, *214*, No. 119012, DOI: 10.1016/j.energy.2020.119012.

(2) Chen, L.; Huang, F.; Li, G.; Mao, Z.; Hu, Y.; Liu, L.; Zeng, H.; Xu, S. Experimental Study on Fiber Balls for Bridging in Fractured-Vuggy Reservoir. *SPE Journal* **2023**, *28* (04), 1880−1894.

(3) Chen, L. F.; Wang, J. J.; Yu, L.; Zhang, Q.; Fu, M. L.; Zhao, Z. C.; Zu, J. Q. Experimental Investigation on the Nanosilica-Reinforcing Polyacrylamide/Polyethylenimine Hydrogel for Water Shutoff Treatment. *Energy Fuels* **2018**, *32* (6), 6650−6656.

(4) Al-Dhafeeri, A. M.; Nasr-El-Din, H. A. Characteristics of high-permeability zones using core analysis, and production logging data. *J. Pet. Sci. Eng.* **2007**, *55* (1−2), 18−36.

(5) Zhang, Y.; Liu, H.; Huang, W.; Liu, Z.; Chang, B. In Identification and Characterization of High Permeability Zones Using Conventional Logging and Production Logging Data: A Case Study of Kela 2 Gas Field, Proceedings of the 2nd International Conference on Green Energy, Environment and Sustainable Development (GEESD2021), 2021.

(6) De Andrade, J.; Sangesland, S. Cement Sheath Failure Mechanisms: Numerical Estimates to Design for Long-Term Well Integrity. *J. Pet. Sci. Eng.* **2016**, *147*, 682−698.

(7) Lian, W.; Li, J.; Xu, D.; Lu, Z.; Ren, K.; Wang, X.; Chen, S. Sealing failure mechanism and control method for cement sheath in HPHT gas wells. *Energy Reports* **2023**, *9*, 3593−3603.

(8) Chen, L. F.; Li, G.; Chen, Y. D.; Zeng, H. Y.; Mao, Z. Q.; Liu, L.; Wang, X. Y.; Xu, S. Y. Thixotropy research of laponite-hydrogel composites for water shutoff in horizontal wells. *J. Pet. Sci. Eng.* **2022**, *208*, No. 109600, DOI: 10.1016/j.petrol.2021.109600.

(9) Chen, L. F.; Qian, Z.; Li, L.; Fu, M. L.; Zhao, H.; Pu, L. P.; Li, G. Synergism of polyvinyl alcohol fiber to hydrogel for profile modification. *Colloids Surf., A* **2019**, *578*, No. 123609.

(10) Raykov, T. Selective Production Possibilities in Order to Stabilise the Crude oil Production in Oil Field Bockstedt. Master's Thesis, 2017.

(11) Cao, B.; Xie, K.; Lu, X.; Cao, W.; He, X.; Xiao, Z.; Zhang, Y.; Wang, X.; Su, C. Effect and mechanism of combined operation of profile modification and water shutoff with in-depth displacement in high-heterogeneity oil reservoirs. *Colloids Surf., A* **2021**, *631*, No. 127673.

(12) Ning, M.; Jia, J.; Guan, S.; Wang, P.; Liu, Y.; Huang, B.; Liu, Q.; Kong, W. Re-Fracturing Technology Research and Application for Low Permeability Reservoirs in Huabei Oilfield. *IOP Conf. Ser.: Earth Environ. Sci.* **2021**, *647* (1), No. 012044.

(13) Xie, K.; Su, C.; Liu, C.; Cao, W.; He, X.; Ding, H.; Mei, J.; Yan, K.; Cheng, Q.; Lu, X. Synthesis and Performance Evaluation of an Organic/Inorganic Composite Gel Plugging System for Offshore Oilfields. *ACS Omega* **2022**, *7* (15), 12870−12878.

(14) Liu, D.; Shi, X.; Zhong, X.; Zhao, H.; Pei, C.; Zhu, T.; Zhang, F.; Shao, M.; Huo, G. Properties and plugging behaviors of smectite-

superfine cement dispersion using as water shutoff in heavy oil reservoir. *Appl. Clay Sci.* **2017**, *147*, 160−167.
(15) Zhao, C.; Hu, X.; Zhang, Y.; Liang, H.; Fang, H.; Zhang, L.; Tang, S.; Zeng, F. Anti-channeling cementing technology for long horizontal sections of shale gas wells. *Natural Gas Industry B* **2018**, *5* (3), 212−218.
(16) Deng, K.; Liu, W.; Liu, B.; Lin, Y.; Singh, A. Repairing force for deformed casing shaping with spinning casing swage and damage behaviour of cement sheath. *Applied Mathematical Modelling* **2019**, *70*, 425−438.
(17) Zhao, L.; Chen, X.; Zou, H.; Liu, P.; Liang, C.; Zhang, N.; Li, N.; Luo, Z.; Du, J. A review of diverting agents for reservoir stimulation. *J. Pet. Sci. Eng.* **2020**, *187*, No. 106734, DOI: 10.1016/j.petrol.2019.106734.
(18) Zhou, H.; Wu, X.; Song, Z.; Zheng, B.; Zhang, K. A review on mechanism and adaptive materials of temporary plugging agent for chemical diverting fracturing. *J. Pet. Sci. Eng.* **2022**, *212*, No. 110256, DOI: 10.1016/j.petrol.2022.110256.
(19) Jia, H.; Niu, C.-C.; Yang, X.-Y. Improved understanding nanocomposite gel working mechanisms: From laboratory investigation to wellbore plugging application. *J. Pet. Sci. Eng.* **2020**, *191*, No. 107214, DOI: 10.1016/j.petrol.2020.107214.
(20) Zhu, H.; Lin, Y.; Zeng, D.; Zhang, D.; Wang, F. Calculation analysis of sustained casing pressure in gas wells. *Petroleum Science* **2012**, *9* (1), 66−74.
(21) Verma, C.; Olasunkanmi, L. O.; Akpan, E. D.; Quraishi, M. A.; Dagdag, O.; El Gouri, M.; Sherif, E.-S. M.; Ebenso, E. E. Epoxy resins as anticorrosive polymeric materials: A review. *React. Funct. Polym.* **2020**, *156*, No. 104741.
(22) Tan, X.; Zhang, J.; Guo, D.; Sun, G.; Zhou, Y.; Zhang, W.; Guan, Y. Preparation, characterization and repeated repair ability evaluation of asphalt-based crack sealant containing microencapsulated epoxy resin and curing agent. *Constr. Build. Mater.* **2020**, *256*, No. 119433, DOI: 10.1016/j.conbuildmat.2020.119433.
(23) Liu, S.; Liu, W.; Qi, B.; Lin, Z.; Li, P.; Wu, C.; Zhang, Q.; Hu, M.; Guo, J. Development and performance evaluation of epoxy resin system for repairing agent. *J. Appl. Polym. Sci.* **2022**, *139* (22), No. 52260.
(24) Leng, G.; Yan, W.; Ge, H.; Deng, J.; Nguu, D. M.; Tan, R.; Han, Y.; Li, Z. In Experimental Study on High-Strength Resin Wellbore Annulus Plugging Technology of Underground Gas Storage Facilities, 56th U.S. Rock Mechanics/Geomechanics Symposium, 2022.
(25) Gong, X.; Liu, Y.; Jia, X.; Shan, G. Decomposition behavior and decomposition products of epoxy resin cured with MeHHPA in near-critical water. *Journal of Wuhan University of Technology-Mater. Sci. Ed.* **2013**, *28* (4), 781−786.
(26) Li, K.; Zhang, L.; Xu, Z. Decomposition behavior and mechanism of epoxy resin from waste integrated circuits under supercritical water condition. *Journal of Hazardous Materials* **2019**, *374*, 356−364.
(27) Oliveux, G.; Dandy, L. O.; Leeke, G. A. Degradation of a model epoxy resin by solvolysis routes. *Polym. Degrad. Stab.* **2015**, *118*, 96−103.
(28) Liu, Y.; Gong, X.; Wu, S.; Li, L. In Decomposition of Epoxy Resin E-44/METHPA by Tetrahydronaphthalene, 2012 International Conference on Biomedical Engineering and Biotechnology, 2012; pp 1304−1306.
(29) Hanaoka, T.; Arao, Y.; Kayaki, Y.; Kuwata, S.; Kubouchi, M. Analysis of nitric acid decomposition of epoxy resin network structures for chemical recycling. *Polym. Degrad. Stab.* **2021**, *186*, No. 109537, DOI: 10.1016/j.polymdegradstab.2021.109537.
(30) Dang, W.; Kubouchi, M.; Sembokuya, H.; Tsuda, K. Chemical recycling of glass fiber reinforced epoxy resin cured with amine using nitric acid. *Polymer* **2005**, *46* (6), 1905−1912.
(31) Liu, Y.; Meng, L.; Huang, Y.; Du, J. Recycling of carbon/epoxy composites. *J. Appl. Polym. Sci.* **2004**, *94* (5), 1912−1916.
(32) Chen, J.; Meng, T.; Wang, Q.; Bai, Y.; Jiaqiang, E.; Leng, E.; Zhang, F.; Liao, G. Study on the mechanisms of epoxy resin gasification in supercritical water by molecular dynamics and experimental methods. *Chem. Eng. J.* **2022**, *433*, No. 133828, DOI: 10.1016/j.cej.2021.133828.
(33) Liu, Y.; Liu, J.; Jiang, Z.; Tang, T. Chemical recycling of carbon fibre reinforced epoxy resin composites in subcritical water: Synergistic effect of phenol and KOH on the decomposition efficiency. *Polym. Degrad. Stab.* **2012**, *97* (3), 214−220.
(34) Piñero-Hernanz, R.; García-Serna, J.; Dodds, C.; Hyde, J.; Poliakoff, M.; Cocero, M. J.; Kingman, S.; Pickering, S.; Lester, E. Chemical recycling of carbon fibre composites using alcohols under subcritical and supercritical conditions. *Journal of Supercritical Fluids* **2008**, *46* (1), 83−92.
(35) Jiang, G. J.; Pickering, S. J.; Lester, E. H.; Turner, T. A.; Wong, K. H.; Warrior, N. A. Characterisation of carbon fibres recycled from carbon fibre/epoxy resin composites using supercritical n-propanol. *Compos. Sci. Technol.* **2009**, *69* (2), 192−198.
(36) Wang, Y. Degradation of Anhydride Cured Epoxy Resin and its Degradation Mechanism. Master thesis, Changchun University Of Technology, 2013.
(37) Zhang, L.; Liu, J.; Nie, W.; Wang, K.; Wang, Y.; Yang, X.; Tang, T. Degradation of anhydride-cured epoxy resin using simultaneously recyclable solvent and organic base catalyst. *Journal of Material Cycles and Waste Management* **2018**, *20* (1), 568−577.
(38) Yan, H.; Lu, C.-X.; Jing, D.-Q.; Hou, X.-L. Chemical degradation of amine-cured DGEBA epoxy resin in supercritical 1-propanol for recycling carbon fiber from composites. *Chin. J. Polym. Sci.* **2014**, *32* (11), 1550−1563.
(39) Anusic, A.; Resch-Fauster, K.; Mahendran, A. R.; Wuzella, G. Anhydride Cured Bio-Based Epoxy Resin: Effect of Moisture on Thermal and Mechanical Properties. *Macromol. Mater. Eng.* **2019**, *304* (7), No. 1900031.
(40) Rusli, A.; Cook, W. D.; Schiller, T. L. Blends of epoxy resins and polyphenylene oxide as processing aids and toughening agents 2: Curing kinetics, rheology, structure and properties. *Polym. Int.* **2014**, *63* (8), 1414−1426.
(41) Ding, X.-M.; Chen, L.; Guo, D.-M.; Liu, B.-W.; Luo, X.; Lei, Y.-F.; Zhong, H.-Y.; Wang, Y.-Z. Controlling Cross-Linking Networks with Different Imidazole Accelerators toward High-Performance Epoxidized Soybean Oil-Based Thermosets. *ACS Sustainable Chem. Eng.* **2021**, *9* (8), 3267−3277.
(42) Seek Rhee, G.; Hee Kim, S.; Sun Kim, S.; Hee Sohn, K.; Jun Kwack, S.; Ho Kim, B.; Lea Park, K. Comparison of embryotoxicity of ESBO and phthalate esters using an in vitro battery system. *Toxicology in vitro: an international journal published in association with BIBRA* **2002**, *16* (4), 443−8.
(43) Kong, X.; Xu, Z.; Guan, L.; Di, M. Study on polyblending epoxy resin adhesive with lignin I-curing temperature. *Int. J. Adhes. Adhes.* **2014**, *48*, 75−79.
(44) Rudawska, A. Mechanical Properties of Epoxy Compounds Based on Bisphenol a Aged in Aqueous Environments. *Polymers* **2021**, *13* (6), 952 DOI: 10.3390/polym13060952.
(45) Levchik, S. V.; Weil, E. D. Thermal decomposition, combustion and flame-retardancy of epoxy resins? a review of the recent literature. *Polym. Int.* **2004**, *53* (12), 1901−1929.
(46) Li, W.; Zhao, H.; Pu, H.; Zhang, Y.; Wang, L.; Zhang, L.; Sun, X. Study on the mechanisms of refracturing technology featuring temporary plug for fracturing fluid diversion in tight sandstone reservoirs. *Energy Science & Engineering* **2019**, *7* (1), 88−97.
(47) Wang, T.; Chen, M.; Wu, J.; Lu, J.; Luo, C.; Chang, Z. Making complex fractures by re-fracturing with different plugging types in large stress difference reservoirs. *J. Pet. Sci. Eng.* **2021**, *201*, No. 108413, DOI: 10.1016/j.petrol.2021.108413.
(48) Shen, M.; Almallahi, R.; Rizvi, Z.; Gonzalez-Martinez, E.; Yang, G.; Robertson, M. L. Accelerated hydrolytic degradation of ester-containing biobased epoxy resins. *Polym. Chem.* **2019**, *10* (23), 3217−3229.
(49) Zhang, X.; Wu, Y.; Chen, X.; Wen, H.; Xiao, S.; Zhang, X. Theoretical Study on Decomposition Mechanism of Insulating Epoxy Resin Cured by Anhydride. *Polymers* **2017**, *9* (8), 341 DOI: 10.3390/polym9080341.

https://doi.org/10.1021/acsomega.3c10034
ACS Omega 2024, 9, 19992−20002